JOURNAL OF COMPUTATIONAL PHYSICS 107, 84-97 (1993)

Particle Loading for a Plasma Shear Layer in a Magnetic Field

D. CAI,* L. R. O. STOREY, AND T. NEUBERT

STAR Laboratory, Stanford University, Stanford, California 94305-4055

Received March 18, 1991

Some new particle loading methods have been developed for use in simulating a plasma shear layer with nonuniform density and temperature in the presence of a magnetic field, especially with a large effective ion gyroradius. The numerical approach to the shear instability with strong velocity shear consists of starting a simulation from a state of equilibrium, perturbing this equilibrium in some way, then observing the linear growth of the perturbation and its ultimate saturation. With the usual particle loading method, it is difficult to reproduce the equilibrium state if the ion gyroradius is not small on the scale of the shear. The reason is that, with nonuniform velocity shear, i.e., with the nonuniform E-field, a particle may have more than one guiding-center, the particle distribution cannot be obtained analytically, and it may need to be evaluated numerically. If an equilibrium state is not achieved in the particle loading, the shear may relax by means of an "artificial instability" in the course of the simulation, obscuring the physics of interest. With the particle loading method here presented, we simulate a shear layer in a state close to equilibrium without having to solve the Vlasov–Boltzmann equation.

1. INTRODUCTION

Recent developments in supercomputers and in the techniques of particle simulation have made possible more realistic numerical experiments on nonuniform plasmas. However, a satisfactory method for loading particles so as to simulate magnetized plasmas with a large effective ion gyroradius and with strong velocity shear had not previously been found, despite the interest in plasma flow across a magnetic field. The general configuration that we are considering is shown in Fig. 1. The presence of velocity shear across a magnetic field corresponds to the E-field as indicated in the figure.

The velocity shears in a magnetic field usually give rise to the low-frequency diocotron instability [1–4] or, in the long-wavelength case, to the so-called Kelvin–Helmholtz (K–H) instability [5–10]. Such velocity shears occur in many areas of plasma physics, for instance: plasma heating in Tokamaks by injecting an intense plasma beam; the interaction of the solar wind with planetary magnetospheres; the behavior of field-aligned plasma flows; plasma beam propagation in the ionosphere; and the influence of the Space Shuttle environment on active space experiments [11].

In connection with the K–H instability, shear flows have been extensively studied in neutral fluids and also in magnetoplasmas under conditions where magnetohydrodynamic (MHD) theory applies [10]. In space plasmas, MHD theory is valid only so long as the spatial scale of the shear is much greater than any of the microscopic lengths characterizing the plasma, such as the Debye length or the electron and ion gyroradii. Otherwise it is essential to use kinetic theory in some form, such as particle simulation.

The general configuration that we consider is shown in Fig. 1. The presence of the E-field corresponding to the sheared flow implies a nonuniform charge density through the shear layer. In this configuration, Pritchett and Coroniti [7] understood the importance of the kinetic equilibria and first tried to start the simulations for the K–H instability in equilibrium by solving the first-order Vlasov equation. They performed the two-dimensional electrostatic particle simulations in a magnetized plasma with an assumed smooth velocity profile and with a large effective ion gyroradius, trying to start them in equilibrium. They used a first-order correction to the Vlasov equation to generate a consistent ion distribution with which to start their simulations. They reported [6, 7] that the initial drift profile of the plasma flow relaxed within one gyroperiod, if the ion gyroradius was an appreciable fraction of the spatial scale of the electric field, which means that their first-order correction to the Vlasov equation does not treat this case adequately. As a result, they obtained much smaller growth rate of the instability in their simulations, compared with the growth rate predicted by the linear cold-plasma theory.

Nishikawa *et al.* [8] used a piece-wise linear approximation instead of a smooth shear profile for their initial loading. They performed the simulations in the weak shear limit $|V_y'(x)/\Omega_{ci}| \ll 1$, where $V_y'(x)$ is the gradient of the $\mathbf{E} \times \mathbf{B}$ drift velocity ($V_y(x)$) and Ω_{ci} is the ion gyrofrequency.

* Present address: Institute of Information Sciences and Electronics, The University of Tsukuba, Tsukuba, Ibaraki 305, Japan. E-mail: cai@is.tsukuba.ac.jp.

0021-9991/93 $5.00

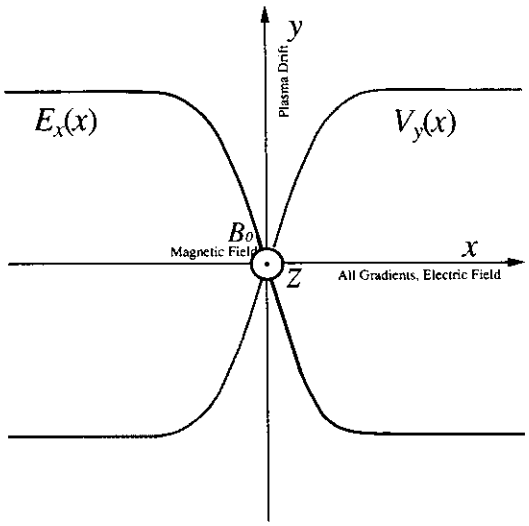

FIG. 1. Schematic diagram of a plasma shear layer at the interface between two moving plasmas in a uniform magnetic field $\mathbf{B}_0$ perpendicular to the direction of motion.

However, no plasma simulations have been done by starting the simulation in equilibrium to see the linear growth of the instability and its proper saturation in a strong shear case with a large effective ion gyroradius, i.e., when $|V_y'(x)/\Omega_{ci}| \geqslant 1$ and $\rho_i/\Delta x \geqslant 0.5$, where ρ_i is the ion gyroradius and Δx is the scale of the shear. Here the effect of the finite ion gyroradius becomes very important and must be taken carefully into account. Many space plasma physics problems involve strong shears; examples are the interactions of the solar wind with planetary magnetospheres and the dynamics of artificial plasma clouds created by active experiments on the Space Shuttle.

Of course, there are many other simulation works where the kinetic aspects of the K–H instability are considered. However, in many of them the simulations are not started in equilibrium, and they are different from our work discussed in the present paper. The differences will be discussed in Section 2B.

The main difficulty in specifying the initial conditions of a plasma with a velocity shear in a magnetic field is that of obtaining the distribution functions of all particle species at an arbitrary point in phase space [12]. The distribution function of a particle is not determined uniquely by the guiding-center of particle, because it may have more than one guiding-center if its gyroradius is not small compared with the spatial scale of the electric field; indeed, a particle can have as many as three guiding-centers if its gyroradius is large enough [12]. Please note here that we define a guiding-center as a point at which $v_y - V_y = 0$, where v_y is the y-component of the particle velocity and V_y is the $\mathbf{E} \times \mathbf{B}$ drift velocity at that point. In the present paper, when the "drift speed" is referred, the $\mathbf{E} \times \mathbf{B}$ velocity is always referred. This is not the same "drift velocity" as the one referred to by this name in the MHD theory, which is defined as the momentum density of the plasma (i.e., the momentum per unit volume) and is almost exactly equal to the local ensemble average velocity of the ions.

As shown in Fig. 1, in our study of the kinetic K–H instability we have limited our attention to its electrostatic limit in the case where the magnetic field is uniform and perpendicular to the velocity of the sheared flow. The main objective of our paper is to present some methods for loading particles into a simulated plasma shear layer in equilibrium with a magnetic field present, when the gyroradius is comparable with the scale of the shear or more than the scale of the shear.

2. PREVIOUS WORKS

A. *Particle Loading*

For a usual particle loading with a spatially uniform plasma with isotropic Maxwellian distribution, it is very common to do the cumulative distribution function solving [13].

For a particle loading with a magnetized and nonuniform plasma without a drift velocity, the difficulty in specifying the initial conditions is discussed by Naitou *et al.* [14] and Birdsall and Langdon [13]. Please note that in the present paper when the "drift speed" is referred, the $\mathbf{E} \times \mathbf{B}$ velocity is referred.

Following the desired equilibrium state, usually only guiding-center positions and velocities can be assigned to the simulation particles. After the particles are loaded in the guiding-center, the actual positions of the particles are determined. However, the resultant actual density $n(x)$ is generally different from the given guiding-center density $N(x)$ if $N(x)$ is spatially nonuniform and the gyroradius is not small compared with the spatial scale of the nonuniformity. Thus, a charge separation occurs for the actual densities due to the difference between the ion and electron gyroradius, when the charge neutrality condition $q_e N_e(x) = q_i N_i(x)$ for the guiding-center densities is required, where q_e and q_i are the electron and ion charges, respectively. N_e and N_i are the guiding-center electron and ion densities, respectively.

Using the Fourier method, Naitou *et al.* [14] discussed two ways to avoid the unwanted charge separation: (1) obtain the guiding-center ion density $N_i(x)$ so that the equilibrium distribution of the actual ion density $n_i(x)$ satisfies $n_i(x) = n_e(x)$, where the equilibrium distribution of the actual electron density $n_e(x) \simeq N_e(x)$ due to small electron gyroradius; and (2) choose the electron density $n_e(x) = n_i(x)$ assuming $n_e(x) \simeq N_e(x)$.

Next, we need to load the particles in the velocity space. Without velocity shear, i.e., without an external E-field, a

well-know equilibrium distribution in a magnetic field is given by

$$f(x, \mathbf{v}) = N(x + v_y/\Omega) \left\{ \frac{m}{2\pi T(x + v_y/\Omega)} \right\}^{3/2} \times \exp\left\{ -\frac{mv^2}{2T(x + v_y/\Omega)} \right\}, \quad (1)$$

where $v = |\mathbf{v}|$, and m, Ω, $N(x)$, and $T(x)$ are the mass, the gyrofrequency, the density at the guiding-center, and the temperature at the guiding-center, respectively. The distribution $f(x, \mathbf{v})$ is the Maxwellian form and the particle loading in velocities is well known [13].

Using the cumulative distribution function, Birdsall and Langdon [13] discussed a similar particle loading method in a magnetic field with a given guiding-center spatial distribution $N_i(x) = 1 + \Delta_i \cos k_0(x + v_y/\Omega_{ci})$, where Ω_{ci} is the ion gyrofrequency, and Δ_i and k_0 are the chosen factors. They assumed electrons are cold and set the electron density to be $n_i(x) = n_e(x)$ so that there are no unwanted potentials due to the charge separation.

With velocity shear that corresponds to an external E-field across a magnetic field, the problem becomes much more complicated than without it. The difficulty of obtaining the equilibrium particle distribution are discussed in our previous paper [12]. The equilibrium particle distribution $f(x, \mathbf{v})$ is no longer the Maxwellian form expressed in (1). As discussed in our previous paper, the equilibrium distribution $f(x, \mathbf{v})$ is in the form of a double integral and needs to be solved numerically. Even if the guiding-center particle density $N(x)$ is uniform, the actual resultant particle density $n(x)$ is different from $N(x)$ as shown in our previous paper [12]. The particle loading cannot be done so easily as Naitou *et al.* [14] and Birdsall and Langdon [13] did, since the equilibrium particle distribution is no longer in the well-known Maxwellian form expressed in (1).

Therefore, in this paper, some new practice loading method will be discussed in Sections 3 and 4 to start a particle simulation in equilibrium with a large effective ion gyroradius. Our loading method will be developed so that we can avoid both the relaxation of the shear by the improper loading [6–8] and the unphysical potential due to the charge separation [13, 14].

B. *Particle Simulations*

There are many previous simulation works where both fluid and kinetic aspects of the K–H instability are considered [6–9, 15–18]. However, not so many particle simulations for the K–H instability are properly started in equilibrium after obtaining the equilibrium distribution of the particle by solving the Vlasov equation in some ways.

Pritchett and Coroniti [7] first tried to start the simulation with smooth velocity shear in equilibrium by solving the first-order Vlasov equation. The work by Ganguli *et al.* [18] came after this. They solved the Vlasov equation and obtained the kinetic equilibria for a small ε, where $\varepsilon = \rho_i/\Delta x$. Nishikawa *et al.* [8] used the kinetic equilibria obtained by Ganguli *et al.* [18] tried to start the simulation in equilibrium. However, their simulation is only good for $\varepsilon \ll 1$. In Sections 3 and 4, a new particle loading method that is good for an arbitrary ε will be discussed.

Except for the above three works, there are many other previous simulation works for the K–H instability, where the simulation is not started in equilibrium. For example, there are previous works by Wagner *et al.* [17] and Theilhaber and Birdsall [15, 16]. They used the artificial macroscopic plasma flow described in Section 2A to generate velocity shear across a magnetic field.

Theilhaber and Birdsall [15, 16] performed a two-dimensional electrostatic particle simulation of plasma-wall sheath to model the plasma behavior in the vicinity of the limiters and walls of magnetized devices. This is done by adding a wall which absorbs all incoming particles and emits none in one side of the boundary of the system and by creating electron–ion pairs spatially at random at each time step.

The electron and ion in each pair are initially created on top of each other, which means $N_e(x) = N_i(x)$, and are given the random Maxwellian velocity. Since the wall exists, the resulting density $n_e(x) \neq n_i(x)$, and the large charge separation in the system occurs. This is the special case of the charge separation discussed by Naitou *et al.* [14]. Then the charge separation in the system generates a plasma shear sheath across a magnetic field and the system becomes unstable. The instability is the kinetic K–H instability.

Theilhaber and Birdsall [15] concluded that the linear fluid theory (small gyroradius, if any) correctly predicted the growth rates of the long-wavelength modes. However, as shown in Fig. 11 of their paper [15], at short- wavelengths, both the maximum growth of the instability and the most unstable wavelength are reduced significantly to half those predicted by the linear fluid theory. Theilhaber and Birdsall interpreted this difference as due to the finite gyroradius stabilization.

Theilhaber and Birdsall [15] started the simulation with a dramatic sheath formation, with a rapid drop in the plasma potential and formation of the large E-field and large shear at the edge of the simulation domain, which were discussed by Naitou *et al.* [14]. However, Theilhaber and Birdsall solved the linear fluid equation numerically from random-noise initial conditions. Then they measured the growth rate of the mode that emerges out of the noises. In Sections 3 and 4, we will discuss the particle loading methods which enable the simulations to be started from a state of equilibrium.

In Wagner *et al.* [17], the electron sheet was given a finite

thickness in the system by loading the guiding-center electrons evenly across the system. Thermal ions were loaded with their guiding-centers on top of the electrons initially with Maxwellian. As discussed in Naitou *et al.* [14], the configuration like Wagner *et al.* [17] had a step function-type nonuniform density distribution across the system and caused a large charge separation that generated a macroscopic plasma flow in the simulation system. As indicated in Theilhaber and Birdsall [15, 16], it took long time ($700\Omega_{ci}$) to reach the equilibrium state using such a particle loading. Such a simulation made by Wagner *et al.* [17] also expected to have a large oscillation in the system [4, 19] and this might cause the aurora arc deformation in their paper [17]. Also this simulation was not started in equilibrium.

3. THEORY

Our numerical approach to the K–H instability in the presence of strong shear consists of starting a simulation from a state of equilibrium, perturbing this equilibrium in some way, observing the linear growth and ultimate saturation of the perturbation, and finally determining the characteristics of the perturbation field in the saturated state for comparison with the results obtained from the MHD theory.

However, an essential preliminary is the determination of a plausible initial equilibrium state for the unstable plasma. In space plasmas, it is reasonable to assume that the plasma is collisionless, because the mean free path of the particles is usually much larger than the anticipated thickness of the shear layer. Then the equilibrium structure of the layer can be determined as a self-consistent solution of the Vlasov equations for the electrons and ions and of the Poisson's equation for the electric field.

The general configuration that we consider in our investigation of unstable shear flow is indicated in Fig. 1. In the present paper, we have restricted our attention to the case where the magnetic field is oriented exactly perpendicular to the flow velocity: $\mathbf{B}_0 = B_0\hat{z}$. To make the problem soluble, it has been simplified by assuming that the shear layer is plane, that all properties of the plasma depend only on the position along an axis (x) perpendicular to the layer, that the magnetic field ($\mathbf{B}_0$) is uniform and in the plane of the layer, and that the drift velocity (V_y) of the plasma is everywhere perpendicular to the magnetic field (see the basic coordinate axes in Fig. 1); granted these assumptions, we assume a one-dimensional symmetry for our particle loading. The profile of the $\mathbf{E}\times\mathbf{B}$ drift velocity V_y (in the y-direction) versus the position has been given the simple form of a hyperbolic tangent: $V_y = v_0 \tanh(x/\Delta x)$, where Δx is a measure of the thickness of the shear layer. This is also the profile of the electric polarization field ($E_x = -E_0 \tanh(x/\Delta x)$), which is perpendicular to the plane of the layer. The characteristic length over which the change in the velocity occurs is Δx.

The most important theoretical task is to determine how to start the simulation in the equilibrium state. If the simulation does not start from equilibrium, the shear will relax immediately and, in so doing, will mask the important physics. Accordingly a theoretical study of the self-consistent equilibrium of a shear layer in a magnetoplasma was undertaken, and a solution has been found that satisfies the governing equations, together with all the assumptions [12]. The solution is analytic, but it is expressed in terms of double integrals that, in general, have to be evaluated numerically. Our initialization process is based on this analytic theory.

Our goal of the simulation of the K–H instability is to start it from an equilibrium state in two dimensions with an arbitrary length of gyroradius ρ_i, which can be nearly equal to or larger than the thickness of the shear layer Δx. The procedure consists of loading the plasma particles into the simulation domain in a way that is statistically consistent with the analytic solution described in [12]. The two-dimensional simulations will be performed in Section 6. However, for our particle loading, we use the one-dimensional symmetry in this section.

We define dx_g as a small interval of distance in the x-direction. Hereafter we define x_g as the coordinate of a point where particles are loaded. A number of particles (ions) equal to $N(x_g)\,\delta x_g$ per unit distance in the y-direction and unit distance in the z-direction is loaded into the x-positions between the limits $x_g - \delta x_g/2$ and $x_g + \delta x_g/2$. Thus $N(x_g)$ is the number of particles per unit volume loaded very near to x_g; this quantity is supposed to be a known function of x_g. At a given point x_g, the particles are loaded with their x-components of velocity having the probability density function

$$p[v_x(x_g)] = \begin{cases} \dfrac{m}{KT(x_g)}\, v_x(x_g) \exp\left[-\dfrac{mv_x^2(x_g)}{2KT(x_g)}\right], \\ \qquad \text{if} \quad v_x(x_g) > 0; \\ 0, \qquad \text{otherwise}, \end{cases} \tag{2}$$

where k is the Boltzmann constant. Equation (2) is a Rayleigh distribution (see, for instance, Bracewell [20]). The y-component of velocity is set equal to $V_y(x_g)$, the local value of the $\mathbf{E}\times\mathbf{B}$ drift velocity. If the electric field as well as the magnetic field were uniform, then, in a frame moving with the drift velocity, the probability distribution of the particle velocity $\mathbf{v}(=(v_x, v_y))$ would be Maxwellian (see Appendix).

At the point $x = x_g$, the total number of particles with their guiding-centers in the range from $x_g - \delta x_g/2$ to $x_g + \delta x_g/2$ and with their x-component of velocity in the range from $v_x - \delta v_x/2$ to $v_x + \delta v_x/2$ is

$$N(x_g)\, p[v_x(x_g)]\, \delta v_x\, \delta x_g. \tag{3}$$

Here we define a guiding-center as a point at which $v_y - V_y = 0$, where v_y is the y-component of the particle velocity and V_y is the $E \times B$ drift velocity at that point. Thus we can specify the initial positions and velocities of the particles statistically by giving the temperature ($T(x_g)$) and the particle density ($N(x_g)$) at x_g. Defining the thermal velocity

$$v_t = \sqrt{kT/m}, \tag{4}$$

at x_g, a Rayleigh distribution is easily generated by the algorithm

$$v_x(x_g) = v_t \sqrt{-2 \ln R}, \tag{5}$$

where R is a random number uniformly distributed between 0 and 1 [13].

We should note here that, loading the particle in the way described above and defining a guiding-center as a point at which $v_y - V_y = 0$, the particle has a guiding-center at x_g. However, with the nonuniform E-field, x_g is just one of the guiding-centers for the particle, and the particle may have other guiding-centers as shifting from x_g [12].

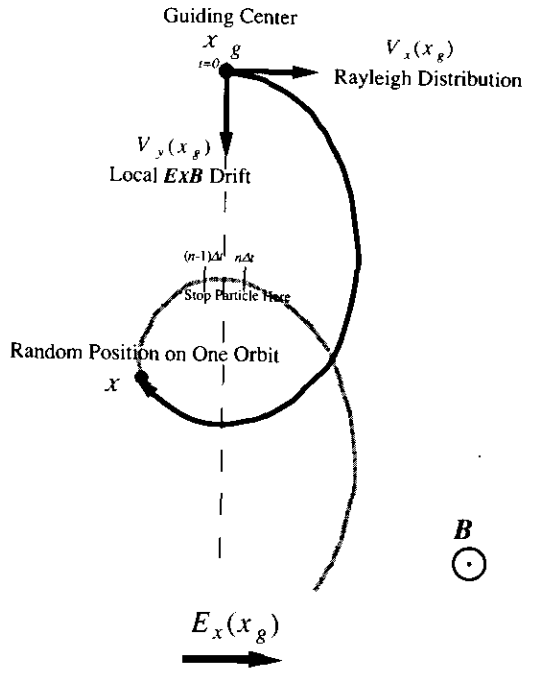

FIG. 2. Guiding-center location. Schematic diagram of our particle loading. A particle is loaded at the loading point x_g and advanced by the Buneman-Boris push.

4. APPLICATION

A. *Ion Loading*

Now we know how to load the particles (ions) at x_g which is the loading point. Next, we need to obtain the particle distribution at an arbitrary point x by shifting the loaded particles from x_g to x under the influence of the polarization electric field, which is fixed. As shown in Fig. 2, first we load a single particle at x_g with velocity components $v_x(x_g)$ picked from a random Rayleigh distribution and $v_y(x_g)$ which is equal to the local $\mathbf{E} \times \mathbf{B}$ drift velocity $V_y(x_g)$. Then we begin to advance it for a random fraction of its orbital period under the influence of the non-uniform electric field, which is fixed.

In the time-stationary situation that we have been considering, all the particles are on orbits for which the variation of the x-coordinate with time is periodic, and we need to know their periods so as to be able to advance the particle for a random fraction of its orbit. The period of orbital gyration, or *gyroperiod*, of a particle would be independent of velocity if there were no electric field present, but in the presence of such a field it depends on the velocity, in general: let us call it $\tau[x_g, v_x(x_g)]$. The gyroperiod τ equals $2 \int_{x_{min}}^{x_{max}} dx/v_x(x)$, but this integral involves singularities and takes a long time to evaluate numerically. Therefore, we prefer to obtain τ by simulating the motion of the particle, as follows: we load a single particle as mentioned in Section 3; we advance it along its orbit using the Buneman–Boris push [13]; we stop as soon as it has completed one gyration, and note the time taken. To obtain the gyroperiod, the time step Δt is chosen to be $\omega_p \Delta t \leqslant 0.1$ and $\omega_c \Delta t \leqslant 0.2$, where ω_p is the plasma frequency and ω_c is the gyrofrequency. In Section 6, we will perform two-dimensional simulations for the K–H instability, where we use the typical time step $\omega_{pe} \Delta t \leqslant 0.25$. Thus, the time step should be small enough to obtain the gyroperiod of the orbit. In order to obtain a more accurate gyroperiod of the orbit, we use the linear interpolation between $t = n\Delta t$ and $t = (n-1)\Delta t$, where $t = n\Delta t$ is the time just passed one gyration and $t = (n-1)\Delta t$ is the time just before one gyration as shown in Fig. 2. By these means, which are illustrated in Fig. 2, we obtain the gyroperiod $\tau(x_g)$ of the particle relatively rapidly and accurately.

Using the obtained gyroperiod, now we can determine the random fraction of one orbital period by multiplying this period by a random number ranging from zero to one. Then we advance the particle again for a random fraction of one orbit. In reality, we do not advance the particle again. We use the phase space trajectory data, which were calculated before to obtain τ, to advance the particle. The random fraction of one orbital period is also linearly interpolated between the two nearest points to the random fraction in the phase space obtained before, so that we can obtain the better particle distribution.

One more important point we have to be careful about in our particle loading at x_g is that, before we start to advance the particle, the initial conditions for the particle velocities at $t = 0$ must be changed to fit in with the leap-frog time

scheme that is used in the Buneman–Boris push. We need to push $\mathbf{v}(0)$ back to $\mathbf{v}(-\Delta t/2)$ using the force calculated at $t=0$. Thus $\mathbf{v}(-\Delta t/2)$ is shown as

$$v_x(-\Delta t/2) = v_x(0)\cos(\Omega_{ci}\Delta t/2),$$
$$v_y(-\Delta t/2) = -v_y(0)\sin(\Omega_{ci}\Delta t/2) + V_y(x_g). \tag{6}$$

After we load a single particle (ion) into the simulation domain, we need to repeat the same procedure and load all the rest of the particles into the simulation domain. The overall ion loading process can be explained as follows: (1) load a single particle at x_g and advance it for a random fraction of one orbit; (2) repeat the process (1) with uniformly varying x but constant y as shown in Fig. 3; (3) repeat the process (2) with uniformly varying y.

In our loading of Fig. 3, the particles are free to go out beyond the boundaries of our simulation domain. Before starting the particle simulation, we show the initial phase space plot of our particle loading in Fig. 4a. Figure 4a is the initial phase space plot of $x-v_y$ when $\rho_i/\Delta x = 1$ and $v_0/\Omega_{ci}\Delta x = 1$. Because the particles can go freely out from the boundaries in the x-direction and no particles come into the simulation domain from beyond the boundaries, asymmetry in the phase space exists at the boundaries of the simulation domain as indicated in Fig. 4a. Therefore, we need to re-inject the particles which go out from the boundaries to eliminate the asymmetry in the phase space shown in Fig. 4a before starting the simulation. Provided that the variation of the polarization electric field is flat enough near the boundaries in x as shown in Fig. 1, we use the inversion

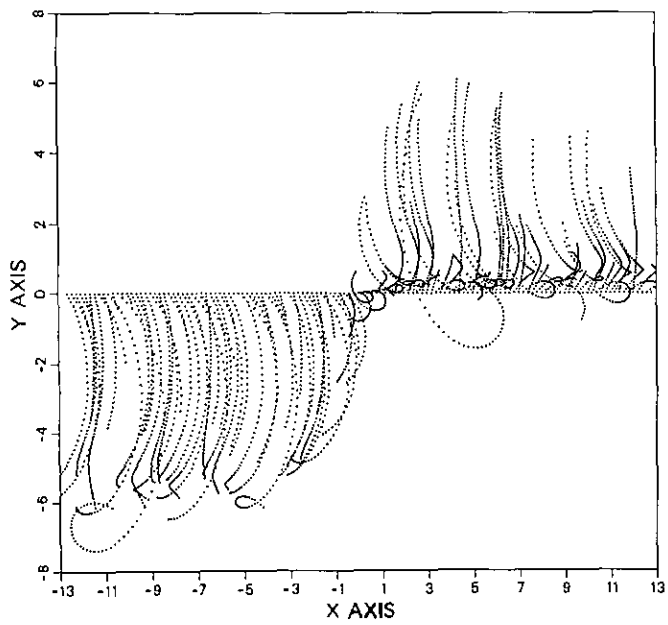

FIG. 3. Particle trajectories for typical initialization. $\Delta x = 1$, $v_0/\Delta x\,\Omega_{ci} = 1$, and $\rho_i/\Delta x = 1$.

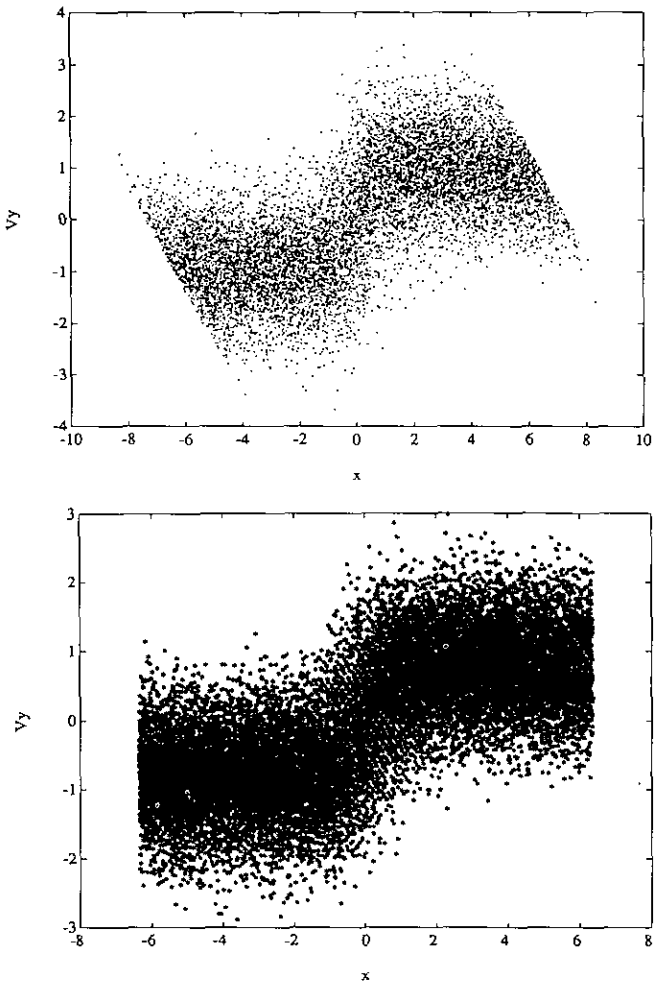

FIG. 4. Phase space plots for our particle loadings: (a) is the initial phase space plot of $x-v_y$ when $\rho_i/\Delta x = 1$; (b) is the initial phase space plot of $x-v_y$ when $\rho_i/\Delta x = 1$ with the inversion symmetry at $x = \pm 6.4$.

symmetry [13] to re-inject the particles which go out from the boundary as shown in Fig. 5. Of course, the loadings are purely one-dimensional and we reserve only x at the boundaries, v_x at 0, and v_y at v_0 in the figure. The origin 0 in Fig. 5 denotes the boundary in x. The result is shown in Fig. 4b.

B. *Electron Loading*

An electron loading is much simpler than ion loading due to its small gyroradius. It is possible for us to use an analytical result developed in our previous report [12] to load electrons.

As discussed in Section 2, without the polarization electric field, the distribution of particle velocity can be simply expressed by the form of $(m/2\pi kT)^{3/2}\exp(-\frac{1}{2}mv^2/kT)$. From our previous paper [12], with a linear polarization field the distribution of the particle velocity still can be expressed by the form of $(m/2\pi kT')^{3/2}\exp(-\frac{1}{2}mv^2/kT')$,

but the temperature is modified to $T' = T/\sqrt{1 + V_y'/\Omega_{ci}}$ and $T/\sqrt{1 - V_y'/\omega_{ce}}$ for ions and electrons, respectively, where ω_{ce} is the electron gyrofrequency. T is the temperature of the particle at the time when they are loaded and that subsequently, as the result of the influence of the electric field, their temperature becomes altered to T'. The modified temperature T' indicates that a positive V_y' leads to a decrease (increase) in ion (electron) temperature and a negative V_y' leads to an increase (decrease) in ion (electron) temperature. Ions (electrons) run away and cannot exist at the loading point when $V_y'/\Omega_{ci} \leqslant -1$ ($V_y'/\omega_{ce} \geqslant 1$). In addition, with a linear electric field, the actual electron density $n_e(x) = N_e(x_g)$, where $N_e(x_g)$ is the guiding-center electron density [12].

Usually the electron gyroradius is much smaller than the spatial scale of the shear (in our simulation we typically use the mass ratio $M_i/m_e = 16$–128). We assume that the electron gyroradius is small enough and the polarization electric field varies linearly in the vicinity of the electron loading point. This assumption is fairly good if we use the first-order particle weighting, or cloud-in-cell model (CIC) in the particle simulation, since we use the electron gyroradius close to one grid spacing Δ in our simulation. Thus we load electrons at x with random velocities characterized by a drifting Maxwellian with modified temperature T'. Note that the electron loading point is x, and not x_g.

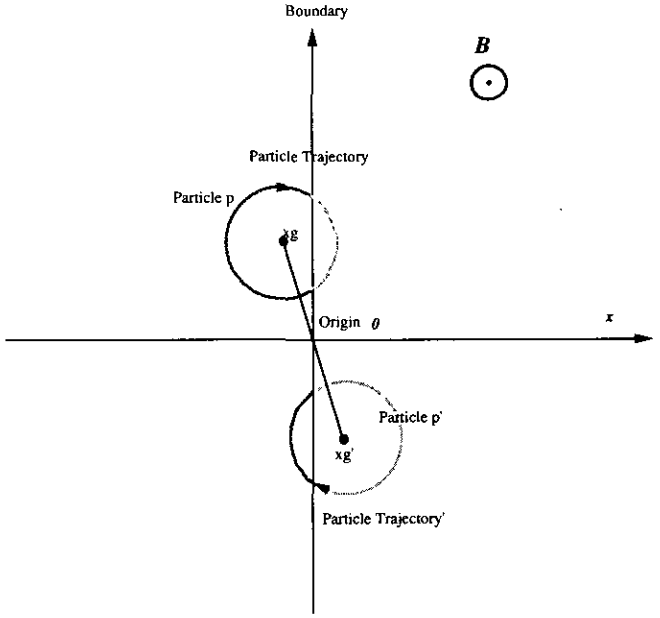

FIG. 5. Inversion symmetry. Schematic diagram of the inversion symmetry used at the boundaries in x for our loadings. We observe the particle p in a frame moving with $v_y = v_0$. The particle has inversion symmetry at $x = 0 = y$, where the origin zero denotes the boundary in x. A particle p going out of the boundary will be re-injected as p' at the boundary with its velocities v_x and v_y reversed at zero and v_0, respectively.

C. *Summary of Particle Loadings*

The ion loading procedure is much more complicated than the electron loading procedure as discussed above. One reason for this is that the ion velocity distribution cannot be explicitly represented by the Maxwellian form due to the large gyroradius. The other reason is that we ignore the difference between the ensemble average particle density and the guiding-center density for the electrons. Our justification for doing this is that the electron gyroradius ρ_e is much smaller than the spatial scale of the shear Δx, and the electric field is varying linearly in the vicinity of the electron loading point. Thus we load the ion at x_g, one of its orbital guiding-centers, with the Rayleigh velocity distribution and advance it for a random fraction of one orbital period under the influence of the tangent hyperbolic electric field as mentioned above.

To sum up, our overall loading procedure can be described as follows: (1) assume a smooth profile for the electric polarization field, hence for the $\mathbf{E} \times \mathbf{B}$ drift velocity; (2) load the ions into the simulation domain with a uniform distribution along the x-axis, which is perpendicular to the plane of the shear layer; (3) give random initial velocities in the positive x-direction with the Rayleigh distribution at the desired temperature to the ions, while in the y-direction then give the local $\mathbf{E} \times \mathbf{B}$ drift velocity; (4) advance each ion along its trajectory, in the presence of the constant but nonuniform electric field, for a random fraction of its orbital period; (5) calculate the ensemble average ion density profile $n_i(x)$ in the way described in our previous paper [12]; (6) calculate the net charge density ρ by the Poisson equation from the electric field given in (1); (7) calculate the electron density $n_e(x)$ by subtracting $\rho/|e|$ from the ion density n_i; (8) load the electrons into the simulation domain in such a way as to yield the required electron density $n_e(x)$; (9) give the electrons random initial velocities with the drifted Maxwellian at the modified temperature $T' = T/\sqrt{1 - V_y'/\omega_{ce}}$.

5. VERIFICATION

The problem now is how to check the correctness of our particle loadings. This is not so simple as one might expect, because in the particle simulation we are dealing with a finite number of discrete particles instead of with continuous statistical quantities. First an electric field varying linearly with x was used to check the algorithm, because in this case an analytic expression can be obtained for the particle distribution as in [12]. The profile of electric field and drift velocity is $E_x(x) = -E_0 x$ and $V_y(x) = v_0 x$, respectively. Figure 6 shows the Maxwell distribution of the particles injected from a single point. To obtain the data graphed in this figure, several thousand (typically 2000) positively charged particles were launched from the same

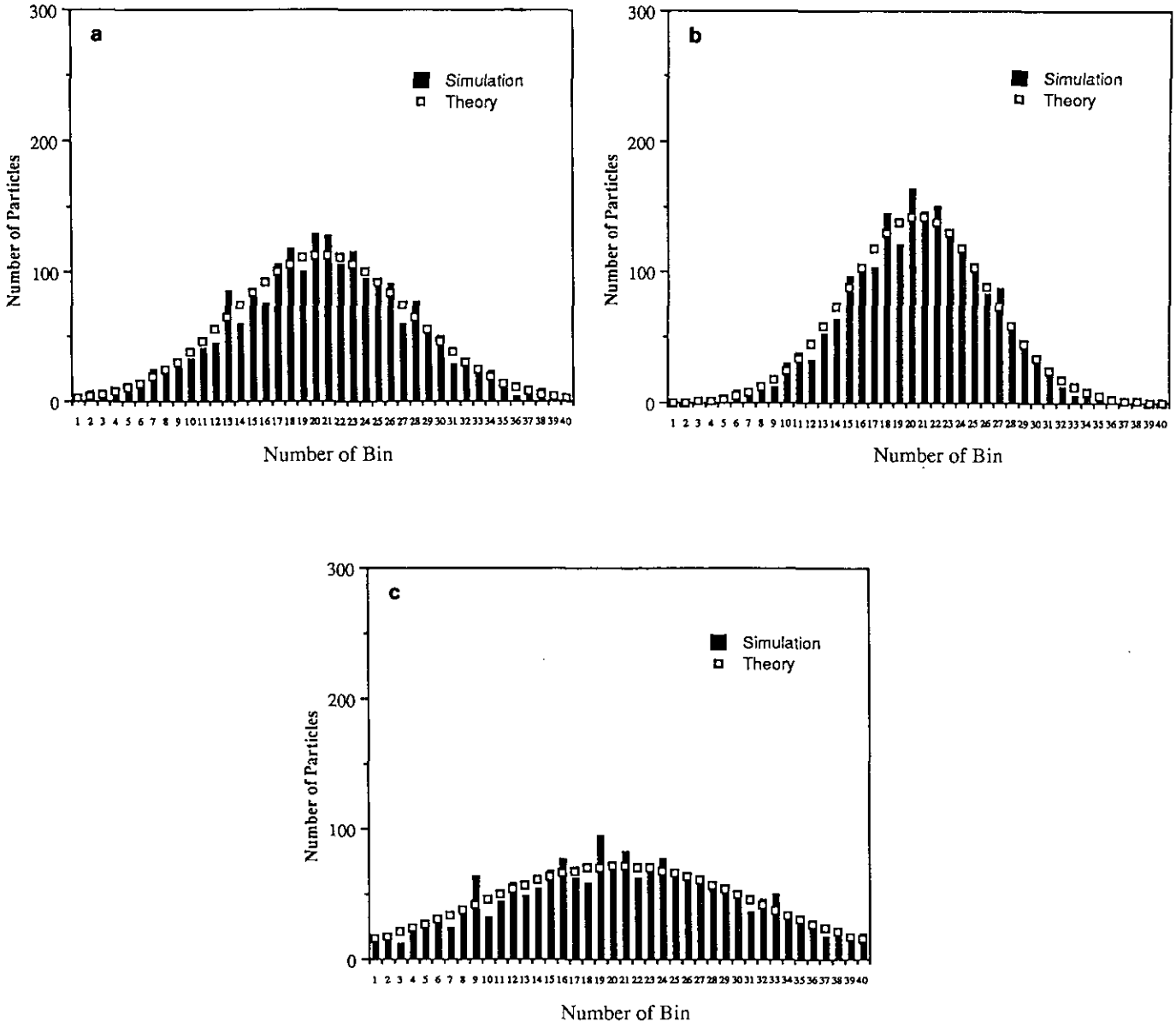

FIG. 6. The Maxwell distribution of the positive particles injected from one point: (a) refers to a case without electric field, where $\rho_i/\Delta x = 1$; (b) refers to a case with the linear electric field, where $v_0 = 0.3$ and $\rho_i/\Delta x = 1$; (c) refers to a case with the linear electric field, where $v_0 = -0.3$ and $\rho_i/\Delta x = 1$.

point on the x-axis, with their velocities chosen by the method described in Section 3. Then they were advanced along their trajectories using the Buneman–Boris push as described in Section 4.

The figures show histograms of the distributions of the final positions of the particles: the launch point, which is the origin of x, is at the interface between bin 20 and bin 21. The x-axis is divided into 40 finite intervals (bins) whose widths are one-tenth of the ion gyroradius. Figure 6a refers to a case with no electric field, and Figs. 6b and c to cases with an electric field linearly proportional to x; the field at each point is directed towards the origin in b, and away from it in c. According to the theory [12], the distributions should be Gaussian in form. Moreover, the Gaussian distribution is wider in the case with a diverging electric field as shown in Fig. 6c, and narrower in the case with a converging electric field as shown in Fig. 6b, than in the case with no field as shown in Fig. 6a, as expected. The open squares in the figures indicate the theoretical Gaussian distributions for this experiment. The numerically simulated distributions match the theoretical ones to within the statistical errors.

The next test is to check the ion density distribution. Even if we load a uniform $N_i(x)$ $(=1)$, the theory predicts that the ion density should vary through the shear layer due to

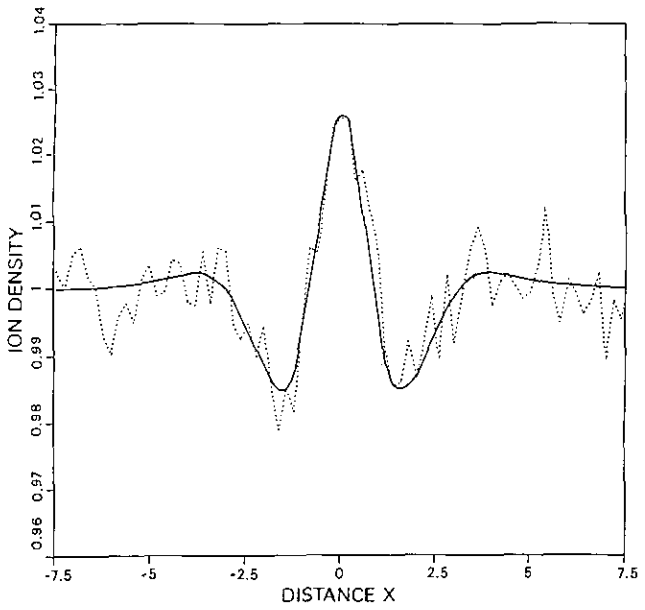

FIG. 7. Ion density distribution. Profiles of the simulated (the dotted line) and the theoretical (the solid line) ion density distribution with the hyperbolic tangent polarization electric field. In all cases, the guiding-center ion density is uniform. The dotted line is the simulated ion density profile in an equilibrium plasma shear layer, where $v_0/\Omega_{ci}\,\Delta x = 1$ and $\rho_i/\Delta x = 2$. The solid line is the theoretical ion density profile in an equilibrium plasma shear layer, where $v_0/\Omega_{ci}\,\Delta x = 1$ and $\rho_i/\Delta x = 2$.

effects of the finite gyroradius, as was explained in our previous paper [12]: in fluid theory the ion density distribution would be flat. The test should be made by determining the density profile numerically, using our particle loading method. Then this simulated profile can be compared with the corresponding one calculated from our analytic theory [12]. Since the initial partial distribution for a 2D simulation has 1D symmetry, the test can be made by a simulation in 1D rather than in 2D. However, for the real particle simulation for the K–H instability, we use a 2D model in Section 6.

In this particle simulation, since we are dealing with a finite number of discrete particles instead of with continuous variables, the profile of ion density exhibits statistical fluctuations, and the sole way to reduce them to an acceptable level is to average over many particles. For instance, for a shear layer with $v_0/\Delta x\,\Omega_{ci} = 1$ and $\rho_i/\Delta x = 2$, the theory predicts that there should be a hump in the ion density of 2.7% at the center of the layer. To see this small variation, we had to average over more than 10,000 particles for one spatial point. The results are given in Fig. 7, where the dotted line shows the ion density distribution from a numerical experiment using our particle loading method, while the solid line shows the corresponding theoretical distribution. There is approximate agreement, inasmuch as each distribution has a peak at the origin flanked by two smaller but somewhat wider troughs, and the dimensions of these features are similar in the two lines; the discrepancies are due to the remaining statistical fluctuations.

6. SIMULATIONS

A. *Model*

To study the kinetic K–H instability we employ a 2D simulation model, in which the fields are functions of both the x and the y coordinates. We restrict our study to the electrostatic limit of the instability, in the case where the magnetic field is uniform and perpendicular to the sheared velocity flow. These simplifications allow us to use a 2D electrostatic particle simulation code.

The main features of our simulations were as follows: they were performed in a slab geometry in which the system was bounded in the x-direction and periodic in the y-direction; the exact particle dynamics were retained for both electrons and ions; particles of both species were reflected at the boundaries; the grid spacing Δ was typically chosen to be equal to the Debye length λ_D; the field equations were solved by the marching method [21] in the x-direction and by the fast Hartley transform method in the y-direction.

In order to prevent the flows generated by the K–H instability from reaching the boundaries, we place the latter at $x = \pm 12.8\,\Delta x$, where Δx is the characteristic length over which the change in the velocity occurs. The system size in the x-direction (L_x) is 25.6 Δx. The characteristic length Δx is chosen to be $5\lambda_D$ in our simulation. Hence the system size in x is $128\lambda_D$. All spatial units on the simulation plots shown in Figs. 8 and 9 are in units of five Debye lengths and one Debye length λ_D equals one grid spacing Δ. In our simulation, we need to choose a small value of the ion to electron mass ratio M_i/m_e, because of the large system size and the large number of particles that are needed for the simulation. Typically we choose the mass ratio M_i/m_e to be 16–128 to enable the simulation runs to be performed in a reasonable time.

Since no kinetic theory of the K–H instability with a large effective ion gyroradius exists, we use the cold-plasma theory or the kinetic theory in the weak shear limits [2, 3, 7] to decide the most unstable mode of the instability. For example, from Fig. 2 of Ref. [7] the normalized wave number $\Delta x\,k_y$ for the most unstable mode it is approximately 0.5. In order to resolve the linear growth of the most unstable mode in the K–H instability, the system size in $y(L_y)$ is chosen to be $64\lambda_D$, which is one wavelength for the most unstable mode. With this system size no more than one most unstable wave can grow and saturate. The average particle density is taken to be $n_0\lambda_D = 16$, so that the total number of particles in the simulation is of order of 260,000.

In each simulation the ions are loaded as mentioned in

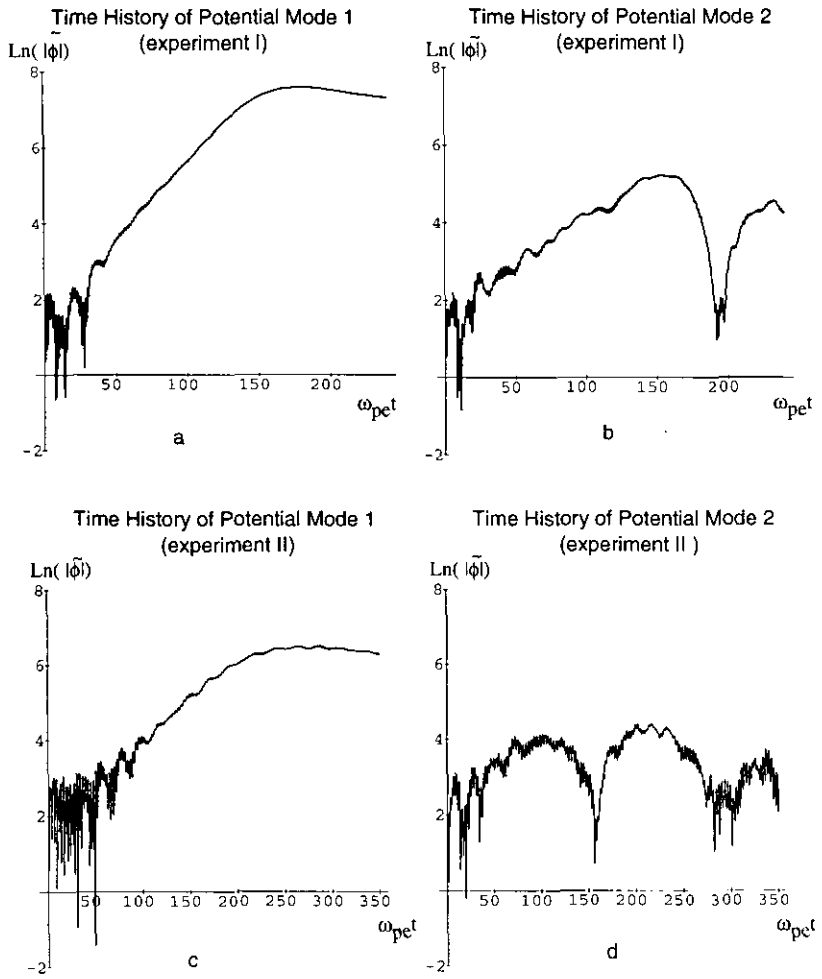

FIG. 8. Time history of the electrostatic potential for modes 1 and 2 in y at the center of the system in the simulation for the Experiments I and II.

Sections 3 and 4, while the electrons are loaded in such a way that the difference between the ion and electron densities yields a space charge corresponding, through Poisson equation, to the assumed profile of the electric field.

B. *Results*

After loading the particles in equilibrium, we are then able to follow the time evolution of the K–H instability. Figure 8 shows the time evolution of the electrostatic potential for the two longest wave modes in y at the center of the system. Mode 1 has dimensionless wave number $k\,\Delta x = 0.49$ and mode 2 has $k\,\Delta x = 0.98$. Thus mode 1 is nearly equal to the most unstable wave mode predicted by the cold-plasma theory. The parameters for Figs. 8a and b are $\rho_i/\Delta x = 0.28$, $\Delta x = 5\lambda_D$, $v_0/\Omega_{ci}\,\Delta x = 1$, $\omega_{pe}/\omega_{ce} = 0.28$, $M_i/m_e = 16$, $(\omega_{pi}/\Omega_{ci})^2 = 4$, and $T_e = T_i$ (Experiment I). The parameters for Figs. 8c and d are $\rho_i/\Delta x = 0.95$, $\Delta x = 5\lambda_D$, $v_0/\Omega_{ci}\,\Delta x = 1$, $\omega_{pe}/\omega_{ce} = 0.5$, $M_i/m_e = 16$, $(\omega_{pi}/\Omega_{ci})^2 = 1.25$, and $T_e = T_i$ (Experiment II). The parameters for both experiments are listed in Table I.

It is apparent from the Figs. 8a and c that the potentials for mode 1 in both experiments grow from their initial states exponentially during the linear stage of the instability and then saturate. These modes show a rapid growth of the K–H instability. For mode 2 and higher-order modes, on the other hand, the growth is significantly reduced or suppressed. From the exponential growth of the potentials for mode 1 in the initial linear stage, we can determine the growth rate of the instability. As shown in Table I, the measured growth rates γ/Ω_{ci} for both experiments are the same and $\gamma/\Omega_{ci} = 0.19$ (note that the estimated uncertainty in the determination of the growth rate is ± 0.02), while the cold-plasma theory predicts $\gamma/\Omega_{ci} = 0.19$ [7].

A uniform time series $\omega_{pe}t = 50$, 100, 150, 200, 250, 300 are shown for Experiment II in Figs. 9 and 10. The initial equilibrium flow obtained by our loading method has no initial perturbation at all so the instability grows from the

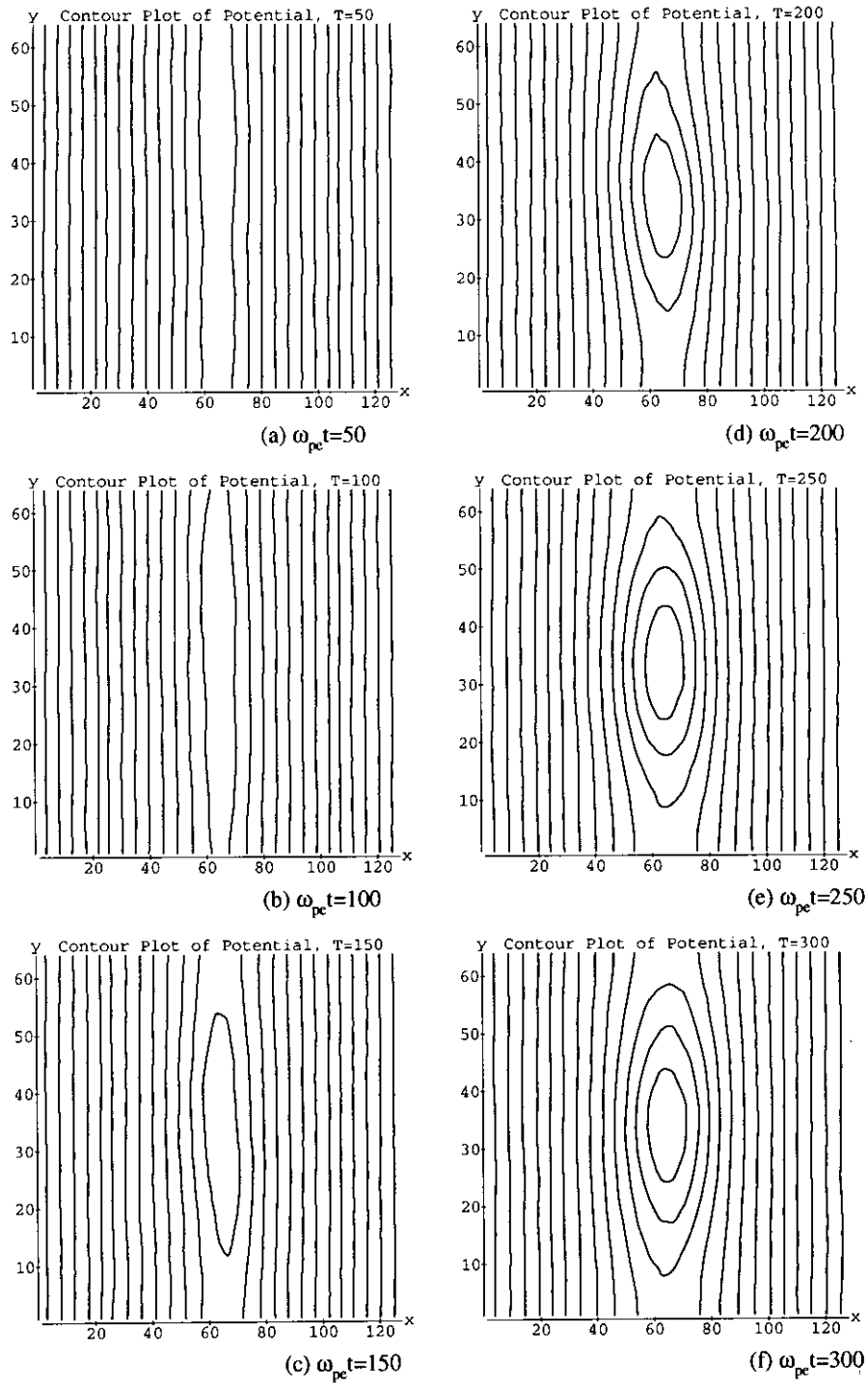

FIG. 9. Evolution of the electrostatic potentials at $\omega_{pe}t = 50$, 100, 150, 200, 250, and 300 for Experiment II.

numerical round-off errors. After the exponential growth, the most unstable mode dominates in frames e and f of Figs. 9 and 10. Figure 9 gives the contours of the electrostatic potentials. In Fig. 10, we show the particle motion in the $x-y$ plane perpendicular to the magnetic field. In Fig. 10, only those particles initially loaded to the left of the $V_y(x) = 0$ symmetry line are darkened.

The interesting point here is the presence of a large island structure in the contour plots of the electrostatic potentials as shown in Fig. 9. The island structure in the potential plots is a characteristic of the K–H instability. At the same time the island is an indicator of the vortex flow produced by the instability. From Fig. 10 we can more clearly see the evolution of the vortices. We first see small tongues of

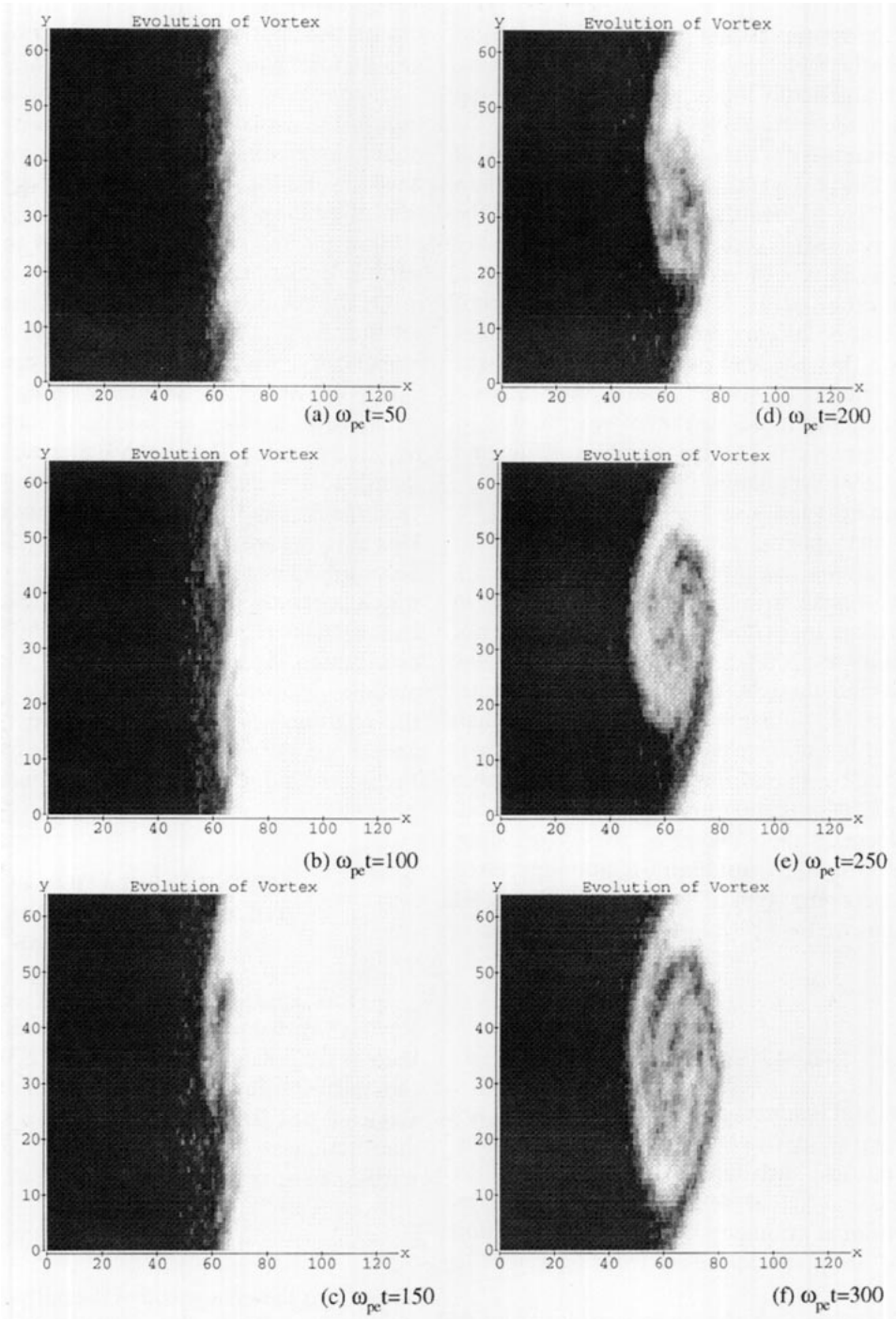

FIG. 10. Evolution of the vortices at $\omega_{pe}t = 50$, 100, 150, 200, 250, and 300 for Experiment II.

TABLE I

Parameters for the Simulations

Experiment	$\rho_i/\Delta x$	Grid spacing Δ	System size L_x	System size L_y	Strength of shear $v_0\Omega_{ci}\Delta x$	ω_{pe}/ω_{ce}	T_i/T_e	M_i/m_e	Growth rate for Mode 1 γ/Ω_{ci}
I	0.28	λ_D	128	128	1	0.28	1	16	~0.19
II	0.95	λ_D	64	64	1	0.5	1	16	~0.19

particles moving across the center line of the simulation domain. Subsequently these tongues grow by combining with the small ones and finally they undergo $\mathbf{E} \times \mathbf{B}$ trapping into one dominant large vortical motion in $x - y$ plane.

One striking feature here is that the K–H instability still grows even if the value of $\rho_i/\Delta x$ is close to one or more than one. Pritchett *et al.* [6, 7] identified their relaxation of the shear as the finite gyroradius stabilization of the instability when the value of $\rho_i/\Delta x$ was close to one or more than one. The reason the relaxation occurs is that, in the particle loading, they use the first-order correction to solve the Vlasov equation, assuming that the shear is small, and start the simulation from a "non-equilibrium" state. If they increase the gyroradius, the equilibrium state cannot be expressed by the simple first-order correction of the distribution function which they used in their simulation [6, 7].

One evidence can be found from Fig. 3 of their paper [7]. The evidence is that before the linear growth of the instability there is a long initial transient period ($400\omega_{pe}$), which we do not observe in our simulation as shown in Fig. 8. During the transient period, the particles that are not loaded in equilibrium are going to adjust themselves to the given electric field and the relaxation of the shear occurs even if Pritchett *et al.* [6, 7] take the value of $\rho_i/\Delta x$ less than one. As listed in Table 1 of their paper [7], when Pritchett *et al.* increase $\rho_i/\Delta x$ close to one or more than one, the shear relaxes and the instability is suppressed. In our simulation, even though we increase the value of $\rho_i/\Delta x$, for example, taking $\rho_i/\Delta x \geqslant 1.0$, the K–H instability is not suppressed and we still observe the typical features of the K–H instability so long as we load the particles in equilibrium.

7. DISCUSSION

The main theoretical contents of our loading method are the relationships that we derive between the guiding-center and the actual particle distributions, and between the guiding-center and the actual densities. The derivations assume one-dimensional symmetry and a known variation of the electric field. It applies to the electrons as well as to the ions.

As we discussed in Section 2, there are two ways to avoid the unwanted charge separation [14]: (1) obtain the guiding-center ion density $N_i(x)$ so that the actual resultant ion density $n_i(x)$ satisfies $n_i(x) = n_e(x)$; and (2) choose $n_e(x) = n_i(x)$, assuming $n_e(x) \simeq N_e(x)$. For our particle loading described in the present paper, we used the latter method.

For no better reason than simplicity, we also assume that the guiding-center density for the ions is known and that it has a given density. For example, we assumed a uniform guiding-center ion density in Sections 4, 5, and 6. It is only on this assumption that all our conclusions regarding the non-uniform equilibrium distribution of ion density applies.

Of course, we can assume that the equilibrium distribution of the actual resultant ion density $n_i(x)$ is given and obtain the guiding-center ion density $N_i(x)$. In this case, we have to load the ions with a certain non-uniform distribution of guiding-center density $N_i(x)$, in such a way as to achieve the required distribution of their actual resultant particle density $n_i(x)$. For this purpose, we are obliged to invert the relationship between $N_i(x)$ and $n_i(x)$. Since this relationship is linear, the inversion is perfectly feasible numerically; it is a sparse matrix inversion.

In point of fact, we should be doing this for electrons. In our particle loading method as it stands, we find $n_e(x)$ is required to create the assumed electric field, and we should then load the electrons with the $N_e(x)$ that is required to yield the required $n_e(x)$ in the presence of the assumed field. However, we assumed that $n_e(x) \simeq N_e(x)$. As discussed in Section 4, in our particle simulation, we use the CIC model which generates the linear electric field over one grid size. In the linear electric field, $n_e(x) = N_e(x)$, and the particle distribution becomes the drifting Maxwellian with the modified temperature [12]. Thus, we do not need to invert the relationship between $n_e(x)$ and $N_i(x)$, so far as we choose the electron gyroradius to be close to one grid size. Indeed, we did so in our particle simulation.

APPENDIX: RELATION BETWEEN THE RAYLEIGH AND MAXWELL DISTRIBUTIONS

In this appendix, we show the relation between the Rayleigh distribution and the Maxwell distribution, when there is no polarization electric field. We demonstrate that the particles loaded at the guiding-center x_g with the Rayleigh distribution will eventually develop the Maxwell distribution at an arbitrary point x. The x-component of particle velocity v_x can be expressed as

$$v_x = v_t \sin(2\pi t/T_g), \tag{A1}$$

where T_g is the gyroperiod of the particle, v_t is the tangential component of particle velocity, and $v_t = v_x(x_g)$. The time derivative of v_x is

$$\frac{dv_x}{dt} = \frac{2\pi v_t}{T_g} \cos\left(\frac{2\pi t}{T_g}\right) = \frac{2\pi}{T_g} v_t \sqrt{1 - \left(\frac{v_x}{v_t}\right)^2}. \tag{A2}$$

Thus we obtain the relation

$$\frac{dt}{dv_x} = \frac{T_g}{2\pi v_t} \frac{1}{\sqrt{1 - (v_x/v_t)^2}}. \tag{A3}$$

As shown in Fig. 11, the particles between the limits $v_x - dv_x/2$ and $v_x + dv_x/2$ spend their time for $2dt$ in one gyroperiod. The probability of finding a particular particle with its velocity in the interval dv_x is

$$p(x_x|v_t)\,dv_x = \frac{2dt}{T_g}, \qquad p(x_x|v_t) = \frac{2}{T_g}\frac{dt}{dv_x}. \tag{A4}$$

From Eqs. (A3) and (A4) the conditional probability density function $p(v_x|v_t)$ which is the probability density of v_x given v_t can be expressed as

$$p(v_x|v_y) = \frac{1}{\pi v_t}\frac{1}{\sqrt{1-(v_x/v_t)^2}}, \quad \text{in} \quad -v_t \leqslant v_x \leqslant v_t. \tag{A5}$$

Thus we have obtained the conditional probability density function $p(v_x|v_t)$. Using the total probability theorem we obtain

$$p(v_x) = \int_{-\infty}^{+\infty} p(v_x|v_t)\,p(v_t)\,dv_t. \tag{A6}$$

Substituting the Rayleigh distribution $p(v_t) = (m/kT)\,v_t \exp[-mv_t^2/2kT]$ and Eq. (A5) into Eq. (A6),

$$p(v_x) = \frac{1}{\pi}\left(\frac{m}{kT}\right)\int_{|v_x|}^{+\infty}\frac{1}{\sqrt{1-(v_x/v_t)^2}}\exp\left[\frac{-mv_t^2}{2kT}\right]dv_t. \tag{A7}$$

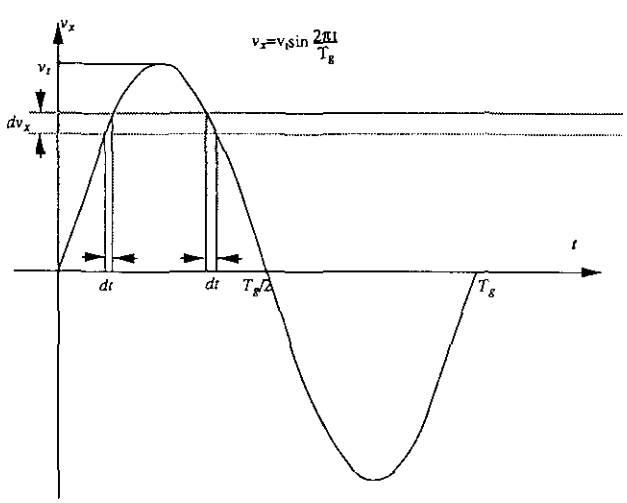

FIG. 11. Schematic diagram of v_x versus t.

What we have to show here is that the equation above is the Maxwell distribution. Let $x = v_t^2/v_x^2$ and $\mu = v_x^2 m/2kT$. We rewrite $p(v_x)$ as

$$p(v_x) = \frac{mv_x}{2\pi kT}\int_1^{+\infty}\frac{\exp(-\mu x)}{\sqrt{x-1}}\,dx. \tag{A8}$$

The integral in the above equation is known and $p(v_x)$ can be written as

$$p(v_x) = \frac{mv_x}{2\pi kT}\sqrt{\frac{\pi}{\mu}}\exp(-\mu) = \sqrt{\frac{m}{2\pi kT}}\exp\left(-\frac{mv_x^2}{2kT}\right). \tag{A9}$$

This completes the proof. Thus $p(v_x)$ is proved to the Maxwell distribution; $p(v_y)$ also can be proved to be the Maxwell distribution using the same procedure mentioned above.

REFERENCES

1. O. Buneman, *Crossed-Field Microwave Devices*, edited by E. Okress (Academic Press, New York, 1961), p. 367.
2. O. Buneman, R. H. Levy, and L. M. Linson, *J. Appl. Phys.* **37**, 3203 (1966).
3. W. Knauer, *J. Appl. Phys.* **37**, 602 (1966).
4. M. Galvetz and C. Barnes, *Phys. Fluids* **31**, 863 (1988).
5. W. I. Axford and C. O. Hines, *Can. J. Phys.* **39**, 1433 (1961).
6. P. L. Pritchett, *Phys. Fluids* **30**, 272 (1987).
7. P. L. Pritchett and F. V. Coroniti, *J. Geophys. Res.* **89**, 168 (1984).
8. K. I. Nishikawa, G. Ganguli, Y. C. Lee, and P. J. Palmadesso, *Phys. Fluids* **31**, 1568 (1988).
9. W. Horton, T. Tajima, and T. Kamiura, *Phys. Fluids* **30**, 3485 (1987).
10. S. Chandrasekhar, *Hydrodynamic and Hydromagnetic Stability* (Clarendon, Oxford, 1961), Chap. 11.
11. D. Cai, T. Neubert, L. R. O. Storey, P. M. Banks, S. Sasaki, K. Abe, and J. L. Burch, *J. Geophys. Res.* **92**, 12451 (1987).
12. D. Cai, L. R. O. Storey, and T. Neubert, *Phys. Fluids B* **2**, 75 (1990).
13. C. K. Birdsall and A. B. Langdon, *Plasma Physics via Computer Simulation* (McGraw-Hill, New York, 1985), pp. 12, 322, 390.
14. H. Naitou, S. Tokuda, and T. Kamimura, *J. Comput. Phys.* **38**, 265 (1980).
15. K. Theilhaber and C. K. Birdsall, *Phys. Fluids B* **1**, 2244 (1989).
16. K. Theilhaber and C. K. Birdsall, *Phys. Fluids B* **1**, 2260 (1989).
17. J. S. Wagner, R. D. Sydra, T. Tajima, T. Hallinan, L. C. Lee, and S.-I. Akasofu, *J. Geophys. Res.* **88**, 8013 (1983).
18. G. Ganguli, Y. C. Lee, and P. J. Palmadesso, *Phys. Fluids* **31**, 823 (1988).
19. D. Cai and O. Buneman, *Phys. Fluids B* **4**, 1033 (1992).
20. R. N. Bracewall, *The Fourier Transform and Its Applications* (McGraw-Hill, New York, 1978), p. 56.
21. O. Buneman, *J. Comput. Phys.* **12**, 124 (1973).